A polymer-based textile thermoelectric generator for wearable energy harvesting

Journal of Power Sources 480 (2020) 228836

Contents lists available at ScienceDirect

Journal of Power Sources

journal homepage: www.elsevier.com/locate/jpowsour

A polymer-based textile thermoelectric generator for wearable energy harvesting

Anja Lund [a,1,*], Yuan Tian [a,1], Sozan Darabi [a,b], Christian Müller [a,b,**]

[a] Department of Chemistry and Chemical Engineering, Chalmers University of Technology, 41296, Göteborg, Sweden
[b] Wallenberg Wood Science Center, Chalmers University of Technology, 412 96, Göteborg, Sweden

HIGHLIGHTS

- E-textiles offer wearable sensing and energy harvesting functionality.
- Thermoelectric energy harvesters can convert body heat to electricity.
- Our thermoelectric textile delivers a record 1.2 μW at $\Delta T = 65$ K.
- Adapted thermoelectric models accurately predict the textile device performance.

GRAPHICAL ABSTRACT

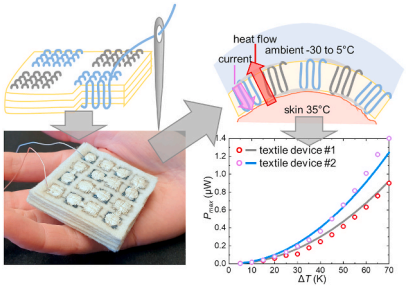

ARTICLE INFO

Keywords:
E-Textiles
Organic electronics
Energy harvesting
Thermoelectrics

ABSTRACT

Conducting polymers offer new opportunities to design soft, conformable and light-weight thermoelectric textile generators that can be unobtrusively integrated into garments or upholstery. Using the widely available conducting polymer:polyelectrolyte complex poly(3,4-ethylenedioxythiophene):poly(styrene sulfonate) (PEDOT:PSS) as the p-type material, we have prepared an electrically conducting sewing thread, which we then embroidered into thick wool fabrics to form out-of-plane thermoelectric textile generators. The influence of device design is discussed in detail, and we show that the performance of e-textile devices can be accurately predicted and optimized using modeling developed for conventional thermoelectric systems, provided that the electrical and thermal contact resistances are included in the model. Finally, we demonstrate a thermoelectric textile device that can generate a, for polymer-based devices, unprecedented power of 1.2 μW at a temperature gradient ΔT of 65 K, and over 0.2 μW at a more modest ΔT of 30 K.

1. Introduction

Electronic textiles (e-textiles) encompass a new class of devices with great potential to transform miniature electronics into truly unobtrusive and ubiquitous systems. Wearable electronics are already part of our daily lives in many forms, ranging from mobile phones and smart watches to pet collars with lights and GPS functionality. Moreover, the use of wearable and even implantable wireless sensors can be expected

* Corresponding author. Department of Chemistry and Chemical Engineering, Chalmers University of Technology, 41296, Göteborg, Sweden.
** Corresponding author. Department of Chemistry and Chemical Engineering, Chalmers University of Technology, 41296, Göteborg, Sweden.
E-mail addresses: anja.lund@chalmers.se (A. Lund), christian.muller@chalmers.se (C. Müller).
[1] These authors contributed equally to the present work.

https://doi.org/10.1016/j.jpowsour.2020.228836
Received 29 May 2020; Received in revised form 12 August 2020; Accepted 23 August 2020
Available online 9 September 2020

to increase rapidly thanks to low power requirements and emerging applications e.g. remote physical condition monitoring and preventive healthcare [1–3]. For uninterrupted and autonomous operation, such devices are ideally powered by energy scavenged from the wearer or from the environment, rather than relying on batteries which will inevitably require replacement. Energy scavenging devices may convert sunlight, biomechanical movement, friction or body heat to electricity relying on photovoltaic, piezoelectric, triboelectric or thermoelectric principles [4]. For wearable devices to be truly unobtrusive, we propose that electronics in the form of textiles are particularly attractive. Several types of e-textile devices for energy harvesting (Fig. 1) have already been reported. In such devices, multi-layer fibers and fabrics function as photovoltaic, piezoelectric or triboelectric energy converters as demonstrated by several groups Refs. [5–7].

Thermoelectric energy harvesters have the advantage of relying on the wearer's natural body heat paired with colder surroundings, without any additional requirements such as motion or available sunlight. For example, commercially available Peltier elements can function as wearable thermoelectric energy scavengers, when placed e.g. on a person's forearm or forehead by means of tape or straps [8–11]. An important conclusion from such studies is that wearable thermoelectric energy harvesting systems will include non-negligible parasitic thermal resistances K_{par}. On the hot side, a thermal contact resistance exists between the rough surface of the skin and the smooth and stiff thermoelectric element. On the cold side, heat rejection relies largely on convection. In standard operation a heat sink, i.e. a block of machined aluminum fins, is attached to the generator *via* thermal paste to increase the surface area available for convection. Clearly, in wearable applications there will exist a trade-off between the size (which is proportional to efficiency) of a heat sink, and the level of discomfort that it causes the wearer.

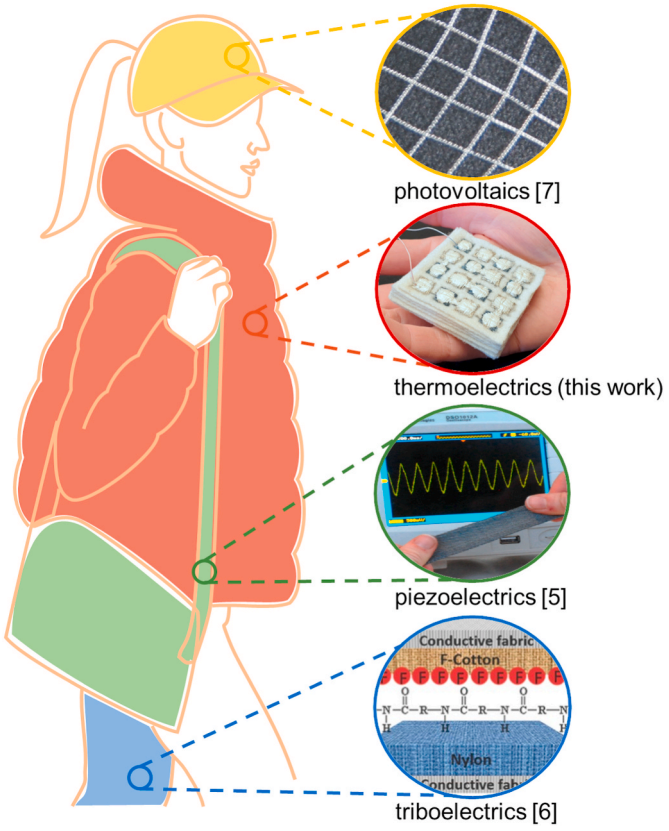

Fig. 1. An overview of the potential use of e-textiles as wearable energy harvesters. The insets show a few examples from literature: (top to bottom) a cap can be sewn from woven solar cell textiles [7] which convert sunlight to electricity, a thick padded jacket can be lined with thermoelectric textiles (example from present work) which convert body heat to electricity, a shoulder bag can be sewn from piezoelectric textiles which convert motion to electricity [5] and a triboelectric weave can be incorporated into a garment in a position where it experiences friction which is then converted to electricity [6]. Insets were adapted and reprinted from Nature Springer under the Creative Commons CC BY license [5], and with permission from Wiley-VCH Verlag GmbH & Co. [6, 7].

The large thermal parasitic resistances result in a system where the device performance is largely dictated by the thermal resistance K_{tc} of the thermocouple, and ideally $K_{tc} \gg K_{par}$. This calls for thermoelectric materials with low thermal conductivity λ. For polymers, λ typically ranges from 0.1 to 0.5 $Wm^{-1}K^{-1}$ [12] (c.f. $\lambda_{air} = 0.025$ $Wm^{-1}K^{-1}$), compared to $\lambda \approx 1.5$ $Wm^{-1}K^{-1}$ [11] for common inorganic thermoelectric materials. Another method to increase the thermal resistance is to increase the device thickness. Consequently, the geometry will play a crucial role for maximized power output. Several studies [9,11,13], which combined comprehensive modeling with experimental work, concluded that for conventional thermoelectric elements used in wearable applications the power output would be optimized by a leg length L much higher than the typical $L = 1$–2 mm. Lossec et al. [13] showed that $L_{optimal} = 55$ mm for a device with all other properties equal to those of a commercial Peltier element based on bismuth telluride alloys. Such a device would be both, too heavy and too brittle for practical use. On the other hand, polymer materials can be readily shaped into light-weight objects of virtually any size [14].

Currently, there exists a strong interest in the materials science community to develop flexible electronics based on conducting polymers. Polymer materials in general display many attractive properties including ease of processing, flexibility, light weight and – crucial for thermoelectric applications – an inherently low thermal conductivity. Moreover, polymers are usually non-toxic, and even biocompatible – a notable example of this is the electrically conducting polymer:polyelectrolyte complex poly(3,4-ethylenedioxythiophene):poly(styrene sulfonate) (PEDOT:PSS) [15]. For thermoelectric applications, a flexible device has the advantage of being conformable to the shape of the human body which can increase the contact area and thus reduce K_{par}. Several doped conjugated polymer systems have been explored as thermoelectric materials [16–20], and they can be converted to textiles by various methods e.g. by coating onto a commercial fabric or by spinning into blend or mono-component fibers. The manufacture and properties of electrically conducting organic textile fibers was described in detail in our recent review paper [21].

Thermoelectric polymer-based textiles can also be prepared by coating a conjugated polymer onto fabric substrates. For example, Du et al. prepared an in-plane device with five thermocouples each consisting of a 35 mm × 5 mm cotton fabric strip coated with PEDOT:PSS and a silver wire [22]. They reported a maximum output power $P_{max} = 12.16$ nW at a temperature gradient $\Delta T = 72$ K, corresponding to 0.03 nW per degree and per leg-pair. Allison et al. used vapor-phase polymerization to deposit p-doped PEDOT (PEDOT-Cl) onto cotton fabrics, and could design an out-of-plane thermoelectric device with two thermocouples, using carbon fiber as the connecting leg, which generated $P_{max} = 4.5$ nW at $\Delta T = 30$ K (0.075 nW per degree and leg-pair) [23]. With one exception, all reports on organic thermoelectric textile devices use PEDOT [22–34] most commonly combined with PSS as the counterion. Pope and Lekakou used poly(3-hexylthiophene) (P3HT) to coat a cotton yarn [30] which was combined with [6,6]-phenyl-C_{61}-butyric acid methyl ester (PCBM) coated n-type yarns and embroidered to form an out-of-plane device with five leg-pairs. The fabricated device produced only $P_{max} = 0.25$ nW at $\Delta T = 40$ K, presumably due to the low electrical conductivity of the yarns.

With this report we would like to draw attention to the potential of e-textiles as out-of-plane thermoelectric devices. We demonstrate the manufacture and characterization of two 3D textile thermoelectric generators, using materials and processes compatible with existing textile manufacture technologies. Our devices have eight thermocouples and generate $P_{max} = 1.2$ μW, at a temperature gradient of 65 K (2.3 nW

per degree and leg-pair). We pay attention to the design considerations, aiming towards optimization of an out-of-plane textile thermoelectric device. We are convinced that our findings will be of interest and practical use to fellow researchers engaged in the development of materials and architectures for e-textile devices.

2. Experimental

2.1. Materials

Approximately 100 m of silk sewing thread (Aurora Silk) was passed through a dye bath prepared with an aqueous PEDOT:PSS dispersion (PH1000 from Heraeus, solid content ~1.3 wt%) and 5 vol% ethylene glycol (EG, from Sigma Aldrich). After collection and drying, the coated thread was placed in a vial containing dimethyl sulfoxide (DMSO, from Sigma Aldrich) for 1 h and 20 min, after which the thread was dried again using a heat gun which heated the air to ~100 °C. This roll-to-roll method for continuous coating and dyeing of conducting threads was developed and previously reported by our group [35]. The second conducting thread used in the thermoelectric devices was a silver-plated polyamide embroidery thread (HC12 from Madeira Garnfabrik).

2.2. Manufacture of thermoelectric textiles

The conducting threads were threaded onto a sewing needle and stitched by hand through 9 layers of felted wool fabric (Wadmal, ~1 mm thick, 3.2 g/dm^2 from Harry Hedgren AB) to form the thermocouple legs. After stitching, a silver-containing paste for textile coatings (PE874 from Dupont) was applied by rubber stamp printing on the surface of the textile to form electrical connections between the respective legs of each thermocouple. After application the paste was cured by placing the embroidered and printed textile in an oven (CARBOLITE PF30/300C) set to 100 °C, for 10 min. A 30 AWG nickel plated copper hookup wire (2930 from Alpha Wire) with heat resistant fluoropolymer insulation was connected to each node of the thermoelectric device, with the aid of silver paste, to serve as connectors to the instruments.

2.3. SEM characterization

Scanning electron microscopy (SEM) was carried out using a JEOL 7800F Prime, at 2 kV. A thin layer of palladium was sputtered onto the samples prior to microscopy.

2.4. Electrical conductivity

For characterization of electrical conductivity, two samples of each thread were placed on a glass slide, and silver paint (Agar Scientific) was applied to form 10 segments each of 8 mm length. The resistance of each length of thread was measured using a Keithley 2400 source meter unit (SMU), and the conductivity was calculated taking into account the thread diameter as observed with an optical microscope (Carl Zeiss A1).

2.5. Seebeck coefficient characterization

The Seebeck coefficient was measured on at least 4 specimens of each thread, using a digital Seebeck controller SB1000 with a temperature controller K2000 (MMR Technologies) and its low impedance board (gain = 1000). Both ends of the ~5 mm long specimen were attached to the holder with silver paint, and a constantan wire was used as a reference. The measurement was performed at 300 K with a thermal load of 1–2 K.

2.6. Specific heat and thermal conductivity

The specific heat capacity c_p was characterized in a DSC2 (Mettler Toledo). Following a blank curve correction run, ~5 mg of each sample and ~10 mg of a sapphire reference material was placed in 40 μl aluminum crucibles, and heated to 80 °C at 20 Kmin^{-1} while recording the heat flow Φ. Using the materials' masses m and the well-defined specific heat capacity of sapphire c_{psap}, we could obtain: $c_p = c_{psap} \cdot (\Phi \cdot m_{sap}) / (m \cdot \Phi_{sap})$. The c_p measured at 23 °C for each material was used as input for the characterization of thermal conductivity, which was carried out with a Hot Disk 2500 S under ambient conditions. This instrument uses a transiently heated plane sensor to simultaneously heat and measure temperature. We characterized our wool fabric, assuming isotropic properties, using a 5465 Kapton sensor sandwiched between 7 + 7 layers of wool fabric (area = 5.3 × 5.3 cm^2) to ensure sufficient volume to accommodate the thermal probing depth. The measurement time was 40 s and heating power 10 mW, resulting in a probing depth of 6 mm. The two electrically conducting threads were expected to display anisotropic characteristics. We prepared rod-like samples from densely packed threads contained in a thermally insulating polypropylene (λ = 0.1–0.2 Wm^{-1}K^{-1}) tube with an inner diameter of 4.7 mm and lengths of 14.5 mm (PEDOT:PSS coated thread) and 22.6 mm (silver plated thread) respectively. The filled tube was placed in a fitted piece of expanded polystyrene (EPS) to prevent lateral heat conduction. A 7577 Kapton sensor (2 mm diameter) was sandwiched between the thread-packed-cylinder and a second piece of EPS. For the PEDOT:PSS dyed silk thread, the measurement time was 40 s and the heating power was 10 mW, resulting in a probing depth of 14.0 mm. For the silver-plated thread, the measurement time was 10 s and the heating power was 25 mW, resulting in a probing depth of 22.5 mm.

2.7. Thermopile characterization

For characterization of the thermoelectric properties of our devices, we placed the thermoelectric textile on top of a variable temperature hot plate (HP60, Torrey Pines Scientific Inc). Surface mounted K-type thermocouples (Omega Engineering) were placed on the top and at the bottom of the textile, to monitor the surface temperatures *via* a National Instruments cDAQ 9174 with internal temperature reference. A repurposed CPU-cooler (Hydro Series™ H45) was placed on top of the thermoelectric textiles to maintain a constant cold temperature of 23 °C. Thin sheets of Kapton (50 μm thickness) were placed on both sides of the textile to prevent electric short circuits. The generated voltage was recorded by a Keithley 2400 SMU, which also acted as a variable load by drawing current from the textiles.

3. Results and discussion

3.1. Thermoelectric device structures and materials

When a conducting or semiconducting material, whether it is metal-, metal oxide-, carbon- or polymer-based, is exposed to a temperature gradient ΔT this will cause a thermal diffusion and subsequent accumulation of charge carriers. This so-called Seebeck effect results in an electric potential difference ΔV in parallel with the ΔT, and the material's Seebeck coefficient α is defined as:

$$\alpha = -\frac{\Delta V}{\Delta T} \tag{1}$$

The direction of the resulting current will depend on the material's majority charge carriers, i.e. electrons or holes, and for a p-type material $\alpha > 0$, while for an n-type material $\alpha < 0$. The smallest unit of a thermoelectric power generator is the thermocouple (tc) (Fig. 2a) constituted of two "legs" – ideally one p-type and one n-type – coupled electrically in series and thermally in parallel so that they both are exposed to the same temperature gradient ΔT_{tc} (Fig. 2b–c). The temperature gradient will result in an open circuit voltage potential V_{tc} over the thermocouple, determined by:

$$V_{tc} = (\alpha_p - \alpha_n)\Delta T_{tc} = \alpha_{tc} \times \Delta T_{tc} \tag{2}$$

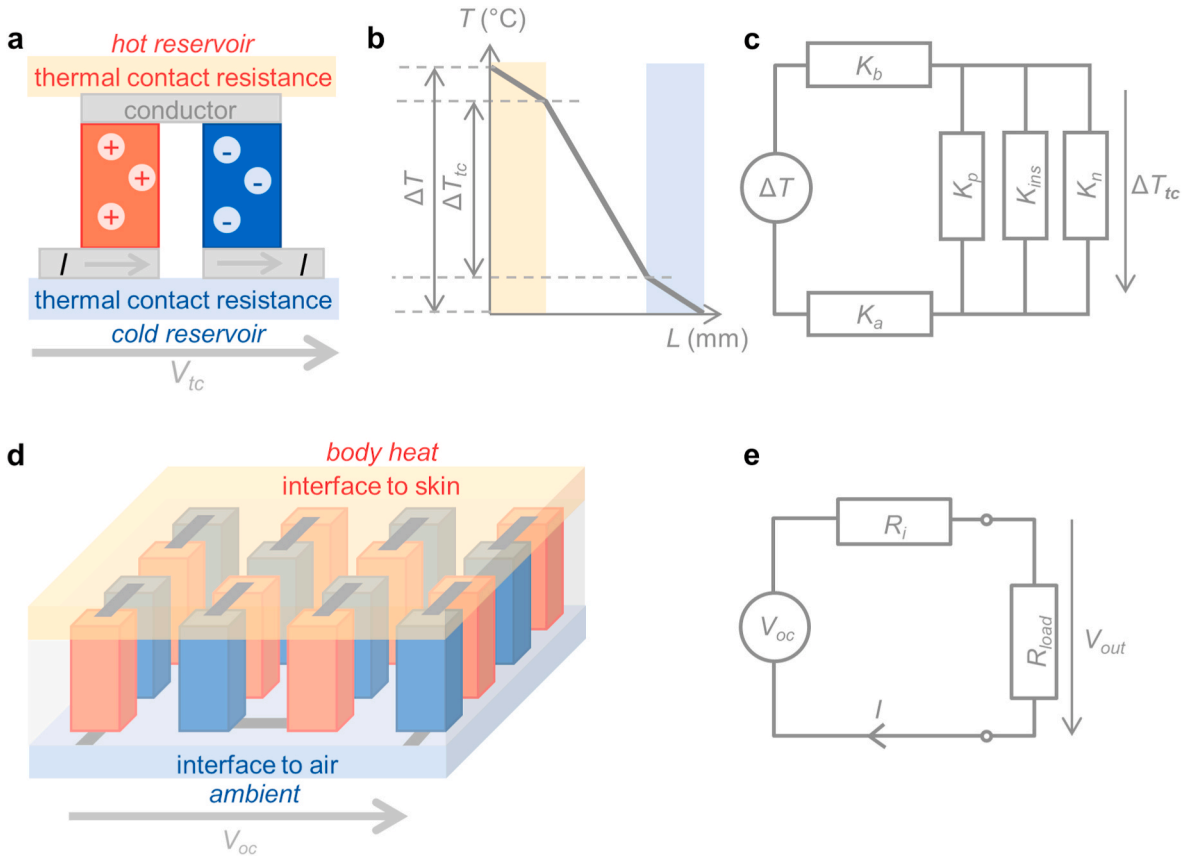

Fig. 2. (a) Schematic representation of a thermocouple (tc) placed between a hot and a cold reservoir. The temperature gradient induces charge carrier diffusion resulting in an electric voltage V_{tc} and a drift current I. The light-blue and light-yellow fields represent thermal contact resistances. (b) The thermal contact resistances introduce a temperature loss resulting in a temperature gradient over the length L of the thermocouple (ΔT_{tc}) which is smaller than the temperature difference (ΔT) between the hot and cold reservoirs. (c) Equivalent circuit representing the thermal resistances in a thermocouple, where K_a and K_b represent the contact resistances on the cold and hot side and K_p, K_n and K_{ins} are the thermal resistances of the p-type, n-type and insulating materials. (d) Schematic representation of a wearable thermopile consisting of several thermocouples connected electrically in series and thermally in parallel. (e) Equivalent electrical circuit of the thermopile where V_{oc} is the open circuit voltage, R_i and R_{load} are the internal resistance and the load resistance, I is the current and V_{out} is the voltage measured at the device terminals. (For interpretation of the references to colour in this figure legend, the reader is referred to the web version of this article.)

where α_p, α_n and α_{tc} are the Seebeck coefficients of the p-type material, the n-type material and of the thermocouple, respectively. Typically, α is on the order of μVK^{-1} so in order to produce a relevant voltage, thermoelectric devices will consist of a number of thermocouples connected in series, forming a thermopile (Fig. 2d). Its maximum produced power P_{max} for a given geometry and under load matching conditions [13], where the internal electrical resistance (R_i) is equal to the load resistance (R_{load}), can be calculated as:

$$P_{max} = \frac{V_{oc}^2}{4R_i} = \frac{(V_{tc} \times m)^2}{4R_i} = \frac{(\alpha_{tc} \times \Delta T_{tc} \times m)^2}{4R_i} \quad (3)$$

where m is the number of thermocouples in the thermopile and V_{oc} is the open circuit voltage of the thermopile (Fig. 2d–e).

To study the feasibility, and predictability, of such a device, we have aimed to use readily available materials and scalable processing methods for its manufacture (Fig. 3a–b). Previously, our group has developed a roll-to-roll method to coat threads with an ink based on the commercially available conducting polymer:polyelectrolyte complex PEDOT:PSS, resulting in a wash-and-wear resistant electrically conducting thread suitable for sewing or weaving [32,35] (Fig. 3a left). PEDOT:PSS displays a Seebeck coefficient in the range of 10–20 μVK^{-1} [22,24,28,30,32,36] and for our thread we measure $\alpha = 14.3\ \mu VK^{-1}$ making it useful as the p-type component of a textile device. At present, no air-stable doped n-type polymers are available. Instead, reported organic n-type textiles have been produced using nanocarbon allotropes i.e. doped carbon nanotubes [29,31,37,38], graphene [39] or PCBM [30]. At present the health and environmental risks related to carbon nanomaterials are under investigation, and notably carbon nanotubes were recently added to the SIN- (Substitute It Now) list developed by ChemSec [40,41]. In the absence of organic n-type materials which are with certainty benign, we opted to use a conducting silver-plated embroidery yarn ($\alpha = 0.3\ \mu VK^{-1}$) to connect the p-type legs in our device. To minimize the electrical contact resistance between p-type and silver-legs, a conducting paste for textile print was used to form electrical connections between thermocouples. By hand-embroidering the threads through several layers of wadmal (a felted wool fabric) we were able to design thick out-of-plane thermoelectric textiles (Fig. 3b), in analogy to a conventional thermopile (Fig. 2d). Thus, the thermocouples were incorporated into an insulating wool fabric and when this is worn on a cold day, the body can constitute a hot reservoir and the colder ambient conditions on the outer side of the garment will provide the cold reservoir. The heat flow from the hot to the cold reservoirs is converted to an electric current, and so this textile device provides warm clothing designed for use in a cold climate, with the added functionality of unobtrusive energy scavenging (Fig. 3c).

3.2. The impact of thermal contact resistance

Under practical conditions there exist thermal contact resistances between a thermocouple and the cold and hot reservoirs, respectively. Assuming conductive heat transfer, the effective ΔT_{tc} driving the

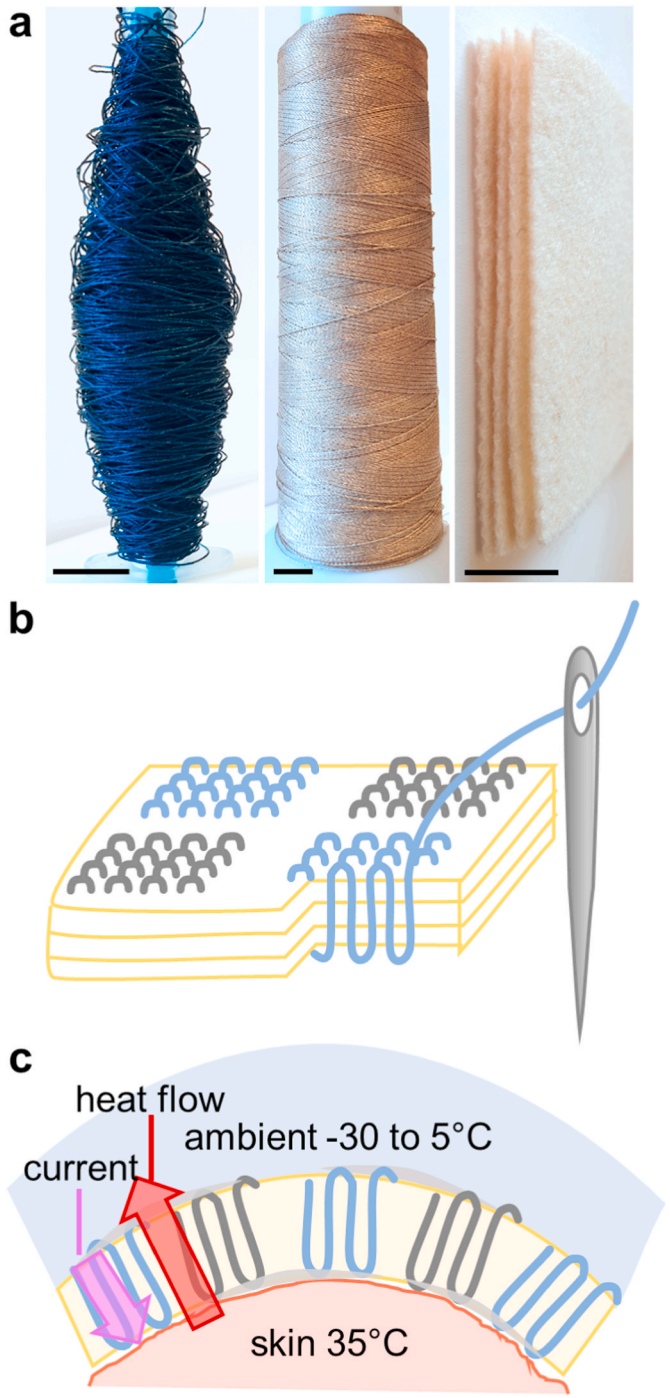

Fig. 3. (a) Photographs of the materials used in our thermoelectric textile: (left) a PEDOT:PSS coated silk thread, (center) a silver plated polyamide thread and (right) several layers of felted wool fabric. Scale bars are 10 mm. (b) Schematic of the embroidery process, showing the position of the threads in a cross-section of the wool fabric. Each cluster of threads represents individual p-type (blue) and n-type (grey) legs. The legs will be electrically connected in series by application of silver paste on the surface of the fabric, to form a thermopile. (c) Schematic illustration of a flexible textile thermopile placed on the skin. The high thickness and low thermal conductivity of the textile ensures its function as an insulator as well as a thermoelectric generator. (For interpretation of the references to colour in this figure legend, the reader is referred to the web version of this article.)

thermoelectric generator can be predicted by:

$$\Delta T_{tc} = \frac{K_{tc}}{K_{tc} + K_a + K_b} \Delta T \tag{4}$$

where ΔT is the available difference in temperature between the hot and cold reservoirs, K_{tc} is the thermal resistance of the thermocouple, and K_a and K_b represent the thermal contact resistances between the generator and the ambient conditions (cold reservoir) and the generator and the body (hot reservoir). In turn, K_{tc} is the combination of the thermal resistances of the p-type material (K_p), the n-type material (K_n) and the thermal insulating material filling the void between the thermocouples (K_{ins}). These thermal resistances can be regarded as coupled in parallel (Fig. 2c), and the resulting K_{tc} is defined by:

$$\frac{1}{K_{tc}} = \frac{1}{K_p} + \frac{1}{K_n} + \frac{1}{K_{ins}} \tag{5}$$

The thermal resistance of a given component is determined by its thermal conductivity λ, its length L and its cross-section area A, as in:

$$K = \frac{L}{\lambda \times A} \tag{6}$$

Likewise, the electrical resistance is defined by a material's electrical conductivity σ and geometry i.e.:

$$R = \frac{L}{\sigma \times A} \tag{7}$$

In addition, electrical contact resistances will be present at all interfaces of the thermocouple. Clearly, the power that a thermoelectric generator can provide is determined not only by material properties but also by geometric considerations. Previously reported wearable thermoelectric generators inevitably have a heatsink attached, and for efficient cooling the devices are positioned so as not to be buried under clothing e.g. on the forehead or on the naked arm [3,9–11,13]. This approach limits the use of wearable devices to warm conditions, resulting in a low available ΔT. Moreover, for a wearable energy harvesting device to be attractive to wear, i.e. to be unobtrusive and comfortable, we propose that the use of conventional heatsinks is simply not an option. Instead, we choose to integrate our device into a textile of low thermal conductivity, and to optimize its geometry (in particular, its thickness) in order to minimize the impact of thermal contact resistances. According to equations (4)–(6), a high $\Delta T_{tc}/\Delta T$ ratio is promoted by:

i. Low thermal contact resistances
ii. Low thermal conductivity of the materials used
iii. A low fill factor (assuming that $K_{ins} < K_{p/n}$)
iv. A large leg length (= device thickness).

Factor (i) is conventionally met by the application of thermal pastes and, on the hot side of the device, aluminum fin heat sinks. Since this is not a viable option for textile wearable devices, we focus instead on the remaining factors. The thermal conductivity λ is defined by thermal diffusivity δ, material density ρ and specific heat c_p as in:

$$\lambda = \delta \rho c_p \tag{8}$$

Because a textile is a porous composite consisting largely of air and some humidity, a textile fabric can display an order of magnitude lower λ compared to its constituent fibers [42]. We have carefully characterized the thermal conductivities of our materials. In our PEDOT:PSS coated silk threads, each thread is composed of many silk filaments placed in parallel along the thread axis, surrounded by the conducting coating (Fig. 4a, left). Our second conducting thread consists of many individual silver-plated polyamide fibers, held together in a 2-ply twist (Fig. 4a, center). Since the textile fibers are aligned (also on a macromolecular scale) we assume that they display anisotropic thermal properties [12]. The thermal gradient in our out-of-plane device will be

parallel to the axis of the threads, consequently we prepared the thread samples for thermal characterization by repeatedly threading them through a polypropylene cylinder (Fig. 4b) until the cylinder was densely filled. For characterization, we placed the sensor on top of this cylinder (Fig. 4c, left) with a thick insulator, in turn, on top of the sensor. The felted wool fabric, instead, consists of textured ('wavy') wool fibers arranged in a random non-woven architecture (Fig. 4a, right). This fabric can be assumed to display isotropic thermal properties and was characterized as a bulk material, with the sensor instead sandwiched between two thick multi-layer wool samples (Fig. 4c, right). We found that for our PEDOT:PSS coated silk thread, $\lambda = 0.18\ \mathrm{Wm^{-1}K^{-1}}$, the silver plated polyamide thread has a higher thermal conductivity of $\lambda = 0.47\ \mathrm{Wm^{-1}K^{-1}}$ and the porous wool fabric displays a low $\lambda = 0.056\ \mathrm{Wm^{-1}K^{-1}}$ (see Table 1 for details). Consequently, factor (ii): low thermal conductivity is fulfilled by our materials.

We chose a design for our embroidered device, which mimics that of conventional thermopiles. In order to generate a high power, the thermopile should ideally have a low internal resistance. Consequently, a high thread count in each thermocouple leg is advantageous, which means that the area of each leg needs to be relatively large. In our device (Fig. 5) we design each leg to be 8 mm by 8 mm, with a spacing of 3–3.5 mm between them to ensure that no electric short circuiting will occur. Our thermopile will have 8 thermocouples connected in series. After initial embroidery trials we found that we can incorporate 133 threads per leg. The total area of each thermocouple (*tc*) will be 11mm x 23 mm = 253 $\mathrm{mm^2}$. Note that each leg will consist of both conducting thread and insulating wool (c.f. Fig. 3b), so in order to calculate the leg cross-section areas we use the thread count N multiplied by the cross-section areas of the n-type and p-type threads, A_n and A_p, respectively. The total area of insulating material per thermocouple $A_{ins} = A_{tc} - N\,(A_p + A_n) = 235\ \mathrm{mm^2}$, and the fill factor $FF = N\,(A_p + A_n)/A_{tc} = 0.07$. In conclusion, a very low fill factor (compared to ~25% for commercial thermopiles [11]), c.f. Point (iii): a low fill factor above, is fully achievable with textiles, as the active components can be embedded in cloth and do not need to be self-supporting.

Moreover, in accordance with point (iv): a large leg length, the textile format is ideal for designing thick devices whereas an inorganic device of > 5 mm thickness would be perceived as heavy and bulky. Textiles are commonly used in centimeter thick configurations, for example in upholstery and mattresses, as well as in outdoor jackets, winter boots and sleeping bags for use in cold climates. The thermal contact resistance K_b between the human body and the thermoelectric module is determined by several factors including the thermal conductivity of the skin, the hardness and the topology of the skin, location on the body and the pressure exerted on the skin by the device. The heat transfer coefficient h_b between the human body and a thermoelectric module has been estimated to be 20 - 100 $\mathrm{Wm^{-2}K^{-1}}$ [11,13,43]. The cold side thermal contact resistance is determined by natural convection

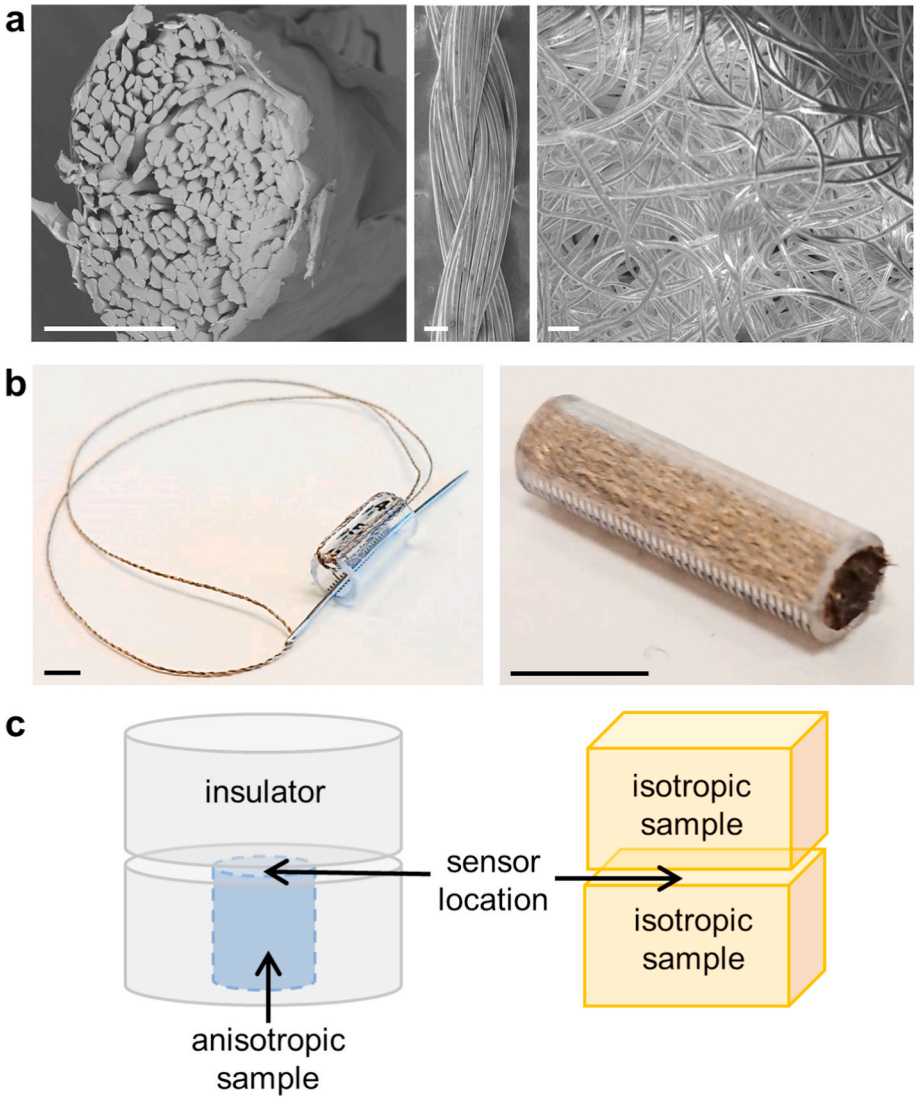

Fig. 4. (a) Scanning electron micrographs of (left) a cross-section of the PEDOT:PSS coated silk thread, displaying the individual silk filaments in the thread, (center) a top view of the silver plated thread and (right) a top view of the wool fabric. Scale bars are 100 μm. (b) Photographs of the sample preparation process for characterization of anisotropic thermal conductivity, where (left) the thread was repeatedly stitched through a polypropylene cylinder to form a (right) rod shaped sample of densely packed threads. Scale bars are 10 mm. (c) Schematic illustrations of the setup for characterization of thermal conductivity of (left) anisotropic samples and (right) isotropic samples.

Table 1
Physical properties: yarn diameter, density (ρ), bulk conductivity (σ_b), Seebeck coefficient (α), specific heat capacity (c_p), thermal diffusivity (δ) and thermal conductivity (λ) of our textile components.

Material	diameter (μm)	ρ (kgm^{-3})	σ_b(Scm^{-1})	α (μVK^{-1})	c_p (Jg^{-1}K^{-1})	δ (mm^{2}s^{-1})	λ (Wm^{-1}K^{-1})
Felted wool	n.a.	290	n.a.	n.a.	1.43	0.14	0.056
PEDOT:PSS coated threads	230	840	43 ± 10	14.3 ± 0.7	1.46	0.14	0.18
Silver-plated threads	350	930	1600 ± 300	0.3 ± 0.1	1.22	0.42	0.47

n.a. = not applicable.

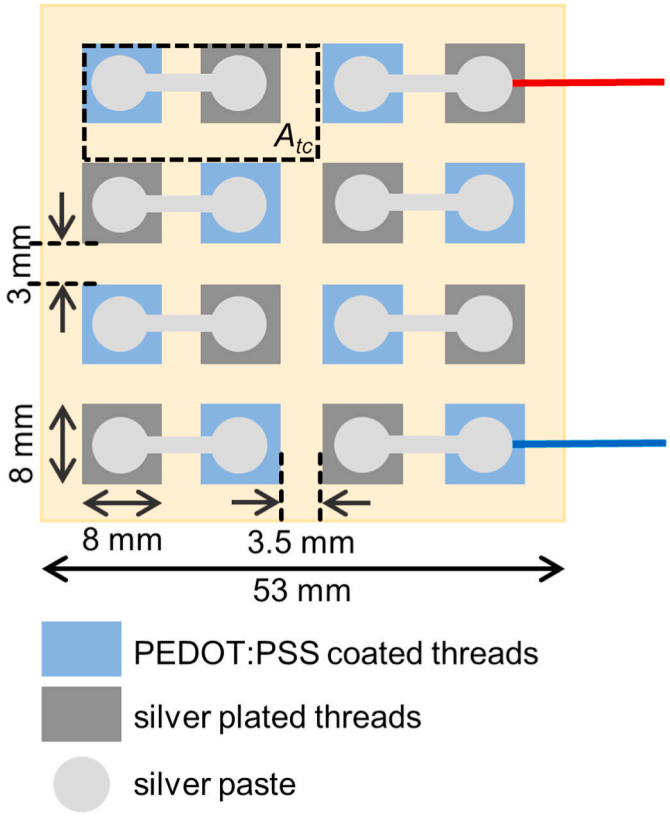

Fig. 5. A schematic outline of a textile thermopile, top view. Silver paste is applied on top of the embroidered textile to form the series electrical connection between thermocouples.

and radiation to the colder environment. The heat transfer coefficient to ambient h_a, without use of a heat sink, is estimated to be relatively low at 6 - 11 Wm^{-2}K^{-1} [13,43]. The heat transfer coefficient relates to the thermal resistance K and the contact area A as in eq. (9):

$$K = \frac{1}{h \times A} \tag{9}$$

Based on the "best case" and "worst case" scenarios from literature we can assume that the contact resistances, per thermocouple, of our textile energy harvester will vary between $(K_a + K_b)_{min} = 390$ KW^{-1} and $(K_a + K_b)_{max} = 860$ KW^{-1}. From the material properties, we use eqs. (5) and (6) to calculate the thermocouple's intrinsic thermal resistance to $K_{tc} = L \times 5{\cdot}10^4$ KW^{-1}.

3.3. The impact of electrical contact resistance

In addition to the intrinsic electrical resistance of our materials, there will exist electrical contact resistances between each leg and thermocouple. We estimate the contact resistance to be about 0.5 Ω per thermocouple. We then proceeded to characterize the bulk electrical conductivity (Table 1) of our threads. It is quite common in e-textile literature to report the surface resistance in terms of Ω□$^{-1}$ or as Scm^{-1} by using an estimated thickness of the conducting layer. We find however that it is more relevant, for the present application, to use the *bulk* volume conductivity (σ_b), therefore we calculate the cross-section area of the conductor using the average thread diameter as observed by optical microscopy. Consequently, a large part of the characterized volume will be constituted by insulating polymer, and σ_b will be relatively low compared to the σ of the conducting component itself (up to $2{\cdot}10^3$ Scm^{-1} for post-treated PEDOT:PSS [36]). To ensure that we access the full circumference of the thread, we apply conducting silver paint at several points along the length of thread samples and measure the electrical resistance between these points, in a two-point configuration. We measure $\sigma_b = 43$ Scm^{-1} for our PEDOT:PSS coated threads, and $\sigma_b = 1600$ Scm^{-1} for the silver plated polyamide threads.

By combining this information with equations (2)–(9), we can predict the generated power as a function of the leg length L, at a given ΔT. We find that the contact resistances, both thermal and electrical, have a significant influence on the predicted thermoelectric voltage and power (Fig. 6). Note that for the purely hypothetical case of zero thermal contact resistance, assuming steady state conditions, L should be as small as possible as this results in minimal internal electrical resistance. However, because the potential difference V_{oc} is proportional to the temperature gradient at the textile boundaries, the addition of thermal contact resistances results in a significantly suppressed electric potential at low L (c.f. eq. (4)). In fact, only at $L > 100$ mm does the open circuit voltage approach the value predicted by (eqs. (2) and (3)) $V_{oc} = (\alpha_p - \alpha_n) \times m \times \Delta T = 14{\cdot}10^{-6} \times 8 \times 65 = 7.28\,mV$ (Fig. 6 a-b, grey lines with triangle symbols) for our device. But as L increases, so does the internal electrical resistance, resulting in a reduction of generated power (Fig. 6 a,b, solid lines). For the most optimistic case in terms of contact resistances (where $h_a + h_b = 111$ Wm^{-2}K^{-1}), $(K_a + K_b)_{min} = 390$ KW^{-1} and the electrical contact resistance is 0.25 Ω per thermopile, the maximum power output P_{max} is found to be 0.8 μW at $L = 15$ mm (Fig. 6b). In our worst case scenario instead where $(h_a + h_b = 26$ Wm^{-2}K^{-1}) the thermal contact resistances are $(K_a + K_b)_{max} = 860$ KW^{-1} and the electric contact resistance is 1 Ω per thermocouple, $P_{max} = 0.3$ μW at the optimal $L = 40$ mm (Fig. 6a). In our lab setup, we may expect the thermal contact resistances to be relatively low and we therefore design our device according to the more optimistic predictions. As embroidery will become increasing difficult with an increasing number of fabric layers, we limit our textile device thickness to 10 mm.

3.4. Characterization of our thermoelectric textile generator

We proceeded to manufacture an out-of-plane thermopile by hand-embroidering our threads through 9 layers of wool fabric. After embroidery, a silver-based conducting coating developed for textiles was used to connect the legs to form an electrical series circuit (Fig. 7a), and two thin copper wires were attached to serve as electrodes. We measured the internal resistance R_i of our device to be 13 Ω. The theoretical value, calculated from geometry and material properties (eq. (7)) would be $R_i = 3.4$ Ω. We conclude that the electrical contact resistance is 1.2 Ω per thermocouple (= 9.6 Ω for the thermopile), which means that the contact resistance is about 3 times higher than the intrinsic resistance of our textile. We proceeded to characterize the thermoelectric performance of our textile by placing it on top of a hot plate, with a repurposed CPU-

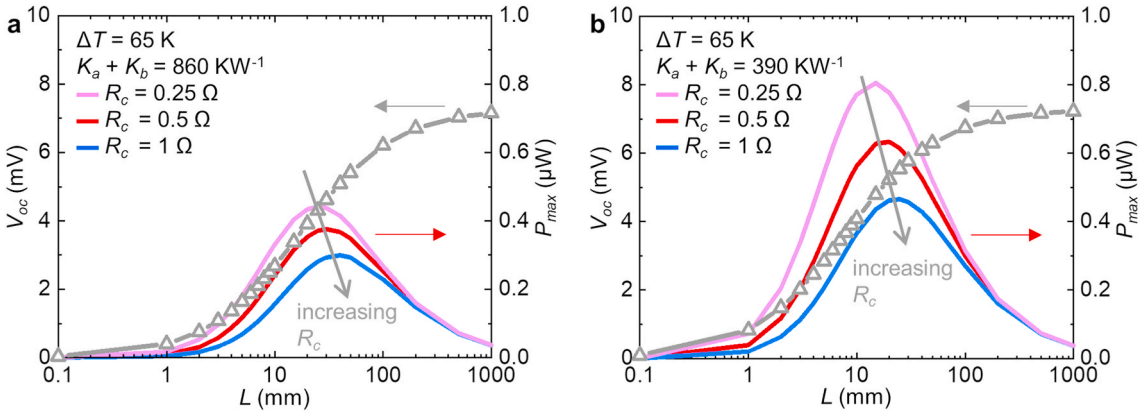

Fig. 6. Predicted open circuit voltage V_{oc} (grey lines with triangle symbols) and predicted maximum power P_{max} (solid lines) generated from our textile thermopile at $\Delta T = 65$ K assuming (a) the worst case thermal resistances $(K_a + K_b)_{max} = 860$ KW^{-1} per thermocouple and (b) the best case thermal contact resistances $(K_a + K_b)_{min} = 390$ KW^{-1} per thermocouple. The electrical contact resistance R_c per thermocouple was 0.25 Ω (purple line), 0.5 Ω (red line) or 1 Ω (blue line). (For interpretation of the references to colour in this figure legend, the reader is referred to the web version of this article.)

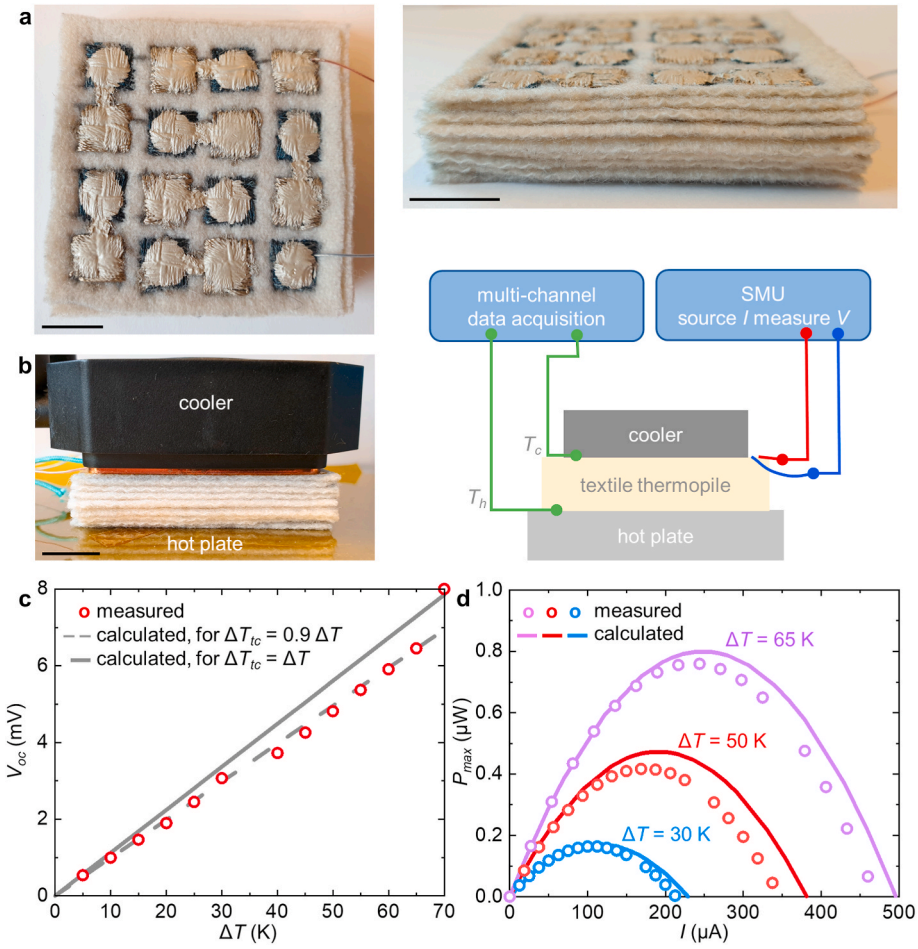

Fig. 7. (a) Photographs of the embroidered textile thermopile, top (left) and side (right) view. (b) Photograph and schematic of the experimental setup for thermoelectric characterization of the thermopile. Scale bars are 10 mm. (c) Experimental results (circles) from the characterization of the open circuit voltage V_{oc} as a function of the temperature gradient ΔT between the hot plate and the cooler, and calculated data for V_{oc} as a function of ΔT where $\Delta T_{tc} = \Delta T$ (solid line) and $\Delta T_{tc} = 0.9 \cdot \Delta T$ (dashed line). (d) Measured generated power (circles) as a function of current, and calculated generated power (solid lines) assuming $\Delta T_{tc} = 0.9 \cdot \Delta T$ and electrical contact resistance = 1.2 Ω per thermocouple. ΔT was 30 K (blue), 50 K (red) and 65 K (purple). (For interpretation of the references to colour in this figure legend, the reader is referred to the web version of this article.)

cooler which holds a constant temperature of 23 °C on top of the textile device (Fig. 7b). We did not apply any thermal paste or other means to enhance thermal contact. We increased the temperature of the hot plate to stepwise increase ΔT and recorded the generated power while drawing an increasing current, i.e. the source-measure unit acted as a variable load to our textile device. The open circuit voltage V_{oc} was taken as the extrapolated voltage at $I \rightarrow 0$. We find that V_{oc} linearly increases with ΔT and is only slightly lower than the V_{oc} predicted by eqs. (2) and (3) (Fig. 7c). From this we could estimate that the ratio of thermal resistances in our setup is $K_{tc}/(K_a + K_b + K_{tc}) \approx 0.9$ which is equal to a $h_a + h_b = 246$ Wm^{-2}K^{-1}. This means that the heat transfer coefficient in our lab setup is about twice as high as that of the "best" wearable system. With this information about the electrical and thermal contact resistances in our system, we could predict the generated power as a function of temperature gradient (Fig. 7d, solid lines), and found that the calculations are a good match with the experimental data

(Fig. 7d, circle symbols).

3.5. A second textile thermopile - leg area optimization

Clearly, the device can be further optimized in several ways. One option is to use the materials more efficiently by taking into account their different electrical conductivities, as previously described by We et al. [44] When the sum $A_n + A_p =$ constant then P_{max} occurs at:

$$\frac{A_n}{A_p} = \sqrt{\frac{\sigma_p \times \lambda_p}{\sigma_n \times \lambda_n}} \tag{10}$$

In our textile device, A_n and A_p are directly proportional to the thread count N of each leg and their respective diameters D, so that:

$$\frac{N_n}{N_p} = \sqrt{\frac{\sigma_p \times \lambda_p}{\sigma_n \times \lambda_n}} \times \left(\frac{D_p}{D_n}\right)^2 = \sqrt{\frac{43 \times 0.18}{1557 \times 0.47}} \times \left(\frac{230}{350}\right)^2 \approx 0.04 \tag{11}$$

Based on this result, we designed a second thermoelectric textile with 8 thermocouples and a thickness of 10 mm, modifying only the thread counts to be $N_p = 398$ and $N_n = 18$ (in the first device $N_p = N_n = 133$), resulting in the device design in Fig. 8a. We manufactured this second device, and measured an internal resistance R_i of 10 Ω whereas according to calculations $R_i = 1.4$ Ω. Again, the internal electrical resistance of our textile device is mainly constituted by contact resistance. We characterized the second device as described previously. As expected, the thermoelectric potential difference again closely follows the predicted V_{oc} in accordance with eqs. (2) and (3) (Fig. 8b), confirming that the thermal contact resistances are of the same magnitude as during the characterization of our first device. The lower internal resistance of our second textile generator resulted in an increase in generated power (Fig. 8c, purple circles), with 1.22 μW generated at $\Delta T = 65$ °C, again a close match to the predicted trend (Fig. 8c, solid blue line).

3.6. Future outlook

The optimization of thermoelectric generators involves a complex relationship between material properties and geometric considerations, and we find it reassuring that traditional calculations, once they have been modified to include thermal and electrical contact resistances, can accurately predict the performance of e-textile devices. In this work, we have not used thermal paste but instead a high device thickness to reduce the negative impact of thermal contact resistances on device performance. Suarez et al. [11] pointed out that thin flexible heat sinks (fin height = 1–3 mm) made from polymers with a thermal conductivity of more than 5 $Wm^{-1}K^{-1}$ could be a viable option for wearable applications, especially when used under windy conditions. Such polymer materials can be manufactured both, from highly aligned polymers as well as by adding fillers to a polymer matrix [12]. We anticipate that future developments of textile thermoelectrics will also include fabrics designed to mimic conventional heat sinks, i.e. with a large surface area.

In addition, the electrical contact resistance has a considerable influence on the power generated. Due to the basic principle of a thermoelectric device, where many legs of different materials are connected in series, electrical contact resistance will always be present in the circuit. Techniques to minimize them warrant further study, e.g. Kirihara et al. [45] reported that the contact resistance at a PEDOT:PSS-metal junction could be significantly reduced by post treatment with EG or DMSO. For the interested reader, we also refer to a recent review paper on interconnects in e-textiles from Agcayazi et al. [46].

4. Conclusions

- E-textile materials can be used to design out-of-plane thermoelectric generators with an unusually large thickness, low fill factor and low thermal conductivity – all of which will increase the thermal gradient over the device.

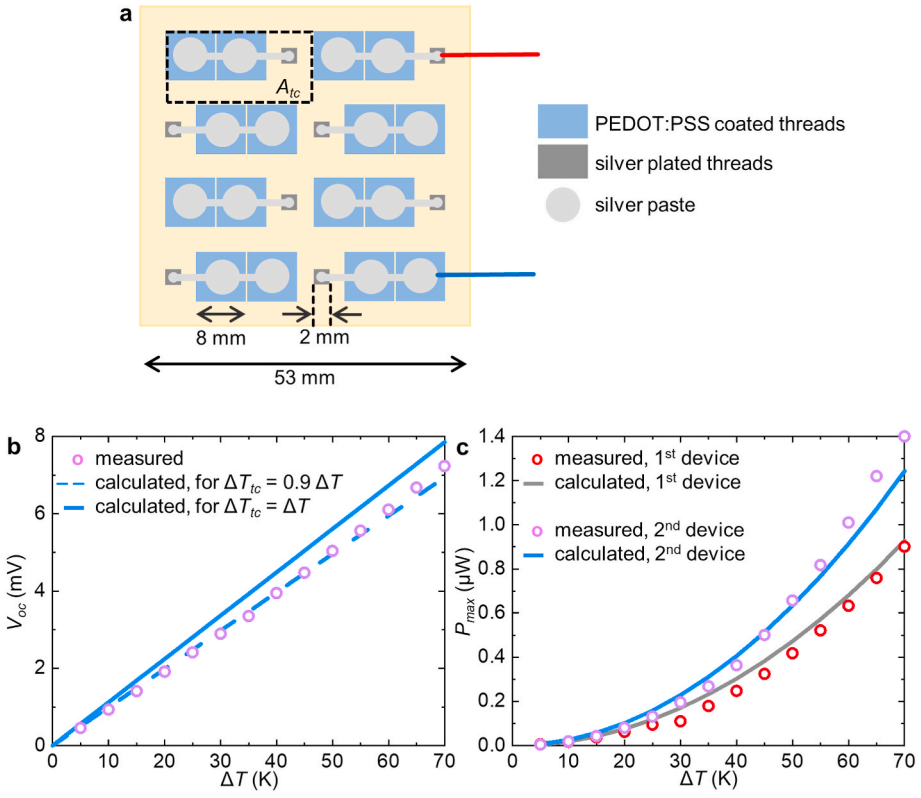

Fig. 8. (a) Schematic outline of our second textile thermopile, with optimized leg areas. (b) Measured open circuit voltage V_{oc} (circles) as a function of the temperature gradient ΔT between the hot plate and the cooler, and calculated data for V_{oc} as a function of ΔT where $\Delta T_{tc} = \Delta T$ (solid line) and $\Delta T_{tc} = 0.9 \cdot \Delta T$ (dashed line). (c) Measured generated power (circles, red for the 1st thermopile, purple for the 2nd thermopile) as a function of ΔT and calculated generated power (solid lines, grey for the 1st thermopile, blue for the 2nd thermopile) assuming $\Delta T_{tc} = 0.9 \cdot \Delta T$ and electrical contact resistance of 1.2 Ω (1st thermopile) or 1.1 Ω (2nd thermopile) per thermocouple. (For interpretation of the references to colour in this figure legend, the reader is referred to the web version of this article.)

- Standard thermoelectric models can be used to accurately predict the performance of e-textile devices, provided that the electrical and thermal contact resistances are included in the model.
- We have used such models to design a thermoelectric textile device which could produce a power >1 μW at $\Delta T = 65$ K, exceeding the previously reported performance achieved by polymer-based textile devices.

Author Statement

A.L. planned the project, developed the instrumentation for textile thermoelectrics characterization, developed the models applied for e-textiles, performed the calculations, wrote the manuscript.

Y.T. manufactured and characterized the textile thermoelectric devices.

S.D. developed the method to manufacture the polymer-based conducting sewing thread, assisted in manufacture and characterization of the materials.

C.M. planned the project, co-wrote the manuscript.

Declaration of competing interest

The authors declare that they have no known competing financial interests or personal relationships that could have appeared to influence the work reported in this paper.

Acknowledgements

This work was performed in part at the Chalmers Material Analysis Laboratory, CMAL. We gratefully acknowledge financial support from the Knut and Alice Wallenberg Foundation through a Wallenberg Academy Fellowship, and the European Research Council (ERC) under grant agreement no. 637624.

References

[1] Y.-W. Chong, W. Ismail, K. Ko, C.-Y. Lee, Energy harvesting for wearable devices: a review, IEEE Sensor. J. 19 (2019) 9047–9062, https://doi.org/10.1109/jsen.2019.2925638.
[2] Z. Lou, L. Wang, K. Jiang, Z. Wei, G. Shen, Reviews of wearable healthcare systems: materials, devices and system integration, Mater. Sci. Eng. R. 140 (2020), 100523, https://doi.org/10.1016/j.mser.2019.100523.
[3] A. Nozariasbmarz, H. Collins, K. Dsouza, M.H. Polash, M. Hosseini, M. Hyland, J. Liu, A. Malhotra, F.M. Ortiz, F. Mohaddes, V.P. Ramesh, Y. Sargolzaeiaval, N. Snouwaert, M.C. Özturk, D. Vashaee, Review of wearable thermoelectric energy harvesting: from body temperature to electronic systems, Appl. Energy 258 (2020), 114069, https://doi.org/10.1016/j.apenergy.2019.114069.
[4] T. Starner, Human-powered wearable computing, IBM Syst. J. 35 (1996) 618–629, https://doi.org/10.1147/sj.353.0618.
[5] A. Lund, K. Rundqvist, E. Nilsson, L. Yu, B. Hagström, C. Müller, Energy harvesting textiles for a rainy day: woven piezoelectrics based on melt-spun PVDF microfibres with a conducting core, npj Flex. Electron. 2 (2018) 9, https://doi.org/10.1038/s41528-018-0022-4.
[6] L. Zhang, Y. Yu, G.P. Eyer, G. Suo, L.A. Kozik, M. Fairbanks, X. Wang, T.L. Andrew, All-textile triboelectric generator compatible with traditional textile process, Adv. Mater. Technol. 1 (2016), 1600147, https://doi.org/10.1002/admt.201600147.
[7] Z. Zhang, Z. Yang, J. Deng, Y. Zhang, G. Guan, H. Peng, Stretchable polymer solar cell fibers, Small 11 (2015) 675–680, https://doi.org/10.1002/smll.201400874.
[8] J.-H. Bahk, H. Fang, K. Yazawa, A. Shakouri, Flexible thermoelectric materials and device optimization for wearable energy harvesting, J. Mater. Chem. C. 3 (2015) 10362–10374, https://doi.org/10.1039/c5tc01644d.
[9] V. Leonov, Thermoelectric energy harvesting of human body heat for wearable sensors, IEEE Sensor. J. 13 (2013) 2284–2291, https://doi.org/10.1109/jsen.2013.2252526.
[10] A.R.M. Siddique, S. Mahmud, B. Van Heyst, A review of the state of the science on wearable thermoelectric power generators (TEGs) and their existing challenges, Renew. Sustain. Energy Rev. 73 (2017) 730–744, https://doi.org/10.1016/j.rser.2017.01.177.
[11] F. Suarez, A. Nozariasbmarz, D. Vashaee, M.C. Öztürk, Designing thermoelectric generators for self-powered wearable electronics, Energy Environ. Sci. 9 (2016) 2099–2113, https://doi.org/10.1039/c6ee00456c.
[12] C. Huang, X. Qian, R. Yang, Thermal conductivity of polymers and polymer nanocomposites, Mater. Sci. Eng. R. 132 (2018) 1–22, https://doi.org/10.1016/j.mser.2018.06.002.
[13] M. Lossec, B. Multon, H. Ben Ahmed, C. Goupil, Thermoelectric generator placed on the human body: system modeling and energy conversion improvements, Eur. Phys. J. Appl. Phys. 52 (2010), 11103, https://doi.org/10.1051/epjap/2010121.
[14] C. Müller, L. Ouyang, A. Lund, K. Moth-Poulsen, M.M. Hamedi, From single molecules to thin film electronics, nanofibers, e-textiles and power cables: bridging length scales with organic semiconductors, Adv. Mater. 31 (2019), e1807286, https://doi.org/10.1002/adma.201807286.
[15] M. Irimia-Vladu, E.D. Głowacki, G. Voss, S. Bauer, N.S. Sariciftci, Green and biodegradable electronics, Mater. Today 15 (2012) 340–346, https://doi.org/10.1016/s1369-7021(12)70139-6.
[16] R. Kroon, D.A. Mengistie, D. Kiefer, J. Hynynen, J.D. Ryan, L. Yu, C. Müller, Thermoelectric plastics: from design to synthesis, processing and structure-property relationships, Chem. Soc. Rev. 45 (2016) 6147–6164, https://doi.org/10.1039/c6cs00149a.
[17] O. Bubnova, X. Crispin, Towards polymer-based organic thermoelectric generators, Energy Environ. Sci. 5 (2012) 9345–9362, https://doi.org/10.1039/c2ee22777k.
[18] Y. Chen, Y. Zhao, Z. Liang, Solution processed organic thermoelectrics: towards flexible thermoelectric modules, Energy Environ. Sci. 8 (2015) 401–422, https://doi.org/10.1039/c4ee03297g.
[19] D. Beretta, A. Perego, G. Lanzani, M. Caironi, Organic flexible thermoelectric generators: from modeling, a roadmap towards applications, Sustain. Energy Fuels 1 (2017) 174–190, https://doi.org/10.1039/c6se00028b.
[20] S.N. Patel, M.L. Chabinyc, Anisotropies and the thermoelectric properties of semiconducting polymers, J. Appl. Polym. Sci. 134 (2016), 44403, https://doi.org/10.1002/app.44403.
[21] A. Lund, N.M. van der Velden, N.-K. Persson, M.M. Hamedi, C. Müller, Electrically conducting fibres for e-textiles: an open playground for conjugated polymers and carbon nanomaterials, Mater. Sci. Eng. R. 126 (2018) 1–29, https://doi.org/10.1016/j.mser.2018.03.001.
[22] Y. Du, K.F. Cai, S.Z. Shen, R. Donelsonand, J.Y. Xu, H.X. Wang, T. Lin, Multifold enhancement of the output power of flexible thermoelectric generators made from cotton fabrics coated with conducting polymer, RSC Adv. 7 (2017) 43737–43742, https://doi.org/10.1039/c7ra08663f.
[23] L.K. Allison, T.L. Andrew, A wearable all-fabric thermoelectric generator, Adv. Mater. Technol. 4 (2019), 1800615, https://doi.org/10.1002/admt.201800615.
[24] Y. Du, K. Cai, S. Chen, H. Wang, S.Z. Shen, R. Donelson, T. Lin, Thermoelectric fabrics: toward power generating clothing, Sci. Rep. 5 (2015) 6411, https://doi.org/10.1038/srep06411.
[25] Y. Du, J. Xu, Y. Wang, T. Lin, Thermoelectric properties of graphite-PEDOT:PSS coated flexible polyester fabrics, J. Mater. Sci. Mater. Electron. 28 (2017) 5796–5801, https://doi.org/10.1007/s10854-016-6250-2.
[26] A.I. Hofmann, I. Östergren, Y. Kim, S. Fauth, M. Craighero, M.-H. Yoon, A. Lund, C. Müller, All-polymer conducting fibers and 3D prints via melt processing and templated polymerization, ACS Appl. Mater. Interfaces 12 (2020) 8713–8721, https://doi.org/10.1021/acsami.9b20615.
[27] Y. Kim, A. Lund, H. Noh, A.I. Hofmann, M. Craighero, S. Darabi, S. Zokaei, J. I. Park, M.H. Yoon, C. Müller, Robust PEDOT:PSS wet-spun fibers for thermoelectric textiles, Macromol. Mater. Eng. 305 (2020), 1900749, https://doi.org/10.1002/mame.201900749.
[28] K. Kirihara, Q. Wei, M. Mukaida, T. Ishida, Thermoelectric power generation using nonwoven fabric module impregnated with conducting polymer PEDOT:PSS, Synthetic Met. 225 (2017) 41–48, https://doi.org/10.1016/j.synthmet.2017.01.001.
[29] J. Liu, Y. Jia, Q. Jiang, F. Jiang, C. Li, X. Wang, P. Liu, P. Liu, F. Hu, Y. Du, J. Xu, Highly conductive hydrogel polymer fibers toward promising wearable thermoelectric energy harvesting, ACS Appl. Mater. Interfaces 10 (2018) 44033–44040, https://doi.org/10.1021/acsami.8b15332.
[30] J. Pope, C. Lekakou, Thermoelectric polymer composite yarns and an energy harvesting wearable textile, Smart Mater. Struct. 28 (2019), 095006, https://doi.org/10.1088/1361-665X/ab1cc1.
[31] J.D. Ryan, A. Lund, A.I. Hofmann, R. Kroon, R. Sarabia-Riquelme, M. C. Weisenberger, C. Müller, All-organic textile thermoelectrics with carbon-nanotube-coated n-type yarns, ACS Appl. Energy Mater. 1 (2018) 2934–2941, https://doi.org/10.1021/acsaem.8b00617.
[32] J.D. Ryan, D.A. Mengistie, R. Gabrielsson, A. Lund, C. Müller, Machine-washable PEDOT:PSS dyed silk yarns for electronic textiles, ACS Appl. Mater. Interfaces 9 (2017) 9045–9050, https://doi.org/10.1021/acsami.7b00530.
[33] H.M. Elmoughni, A.K. Menon, R.M.W. Wolfe, S.K. Yee, A textile-integrated polymer thermoelectric generator for body heat harvesting, Adv. Mater. Technol. 4 (2019), 1800708, https://doi.org/10.1002/admt.201800708.
[34] L. Wang, K. Zhang, Textile-based thermoelectric generators and their applications, Energy Environ. Mater. 3 (2020) 67–79, https://doi.org/10.1002/eem2.12045.
[35] A. Lund, S. Darabi, S. Hultmark, J.D. Ryan, B. Andersson, A. Ström, C. Müller, Roll-to-roll dyed conducting silk yarns: a versatile material for e-textile devices, Adv. Mater. Technol. 3 (2018), 1800251, https://doi.org/10.1002/admt.201800251.
[36] R. Sarabia-Riquelme, M. Shahi, J.W. Brill, M.C. Weisenberger, Effect of drawing on the electrical, thermoelectrical, and mechanical properties of wet-spun PEDOT:PSS fibers, ACS Appl. Polym. Mater. 1 (2019) 2157–2167, https://doi.org/10.1021/acsapm.9b00425.
[37] M. Ito, T. Koizumi, H. Kojima, T. Saito, M. Nakamura, From materials to device design of a thermoelectric fabric for wearable energy harvesters, J. Mater. Chem. A. 5 (2017) 12068–12072, https://doi.org/10.1039/c7ta00304h.
[38] T. Sun, B. Zhou, Q. Zheng, L. Wang, W. Jiang, G.J. Snyder, Stretchable fabric generates electric power from woven thermoelectric fibers, Nat. Commun. 11 (2020) 572, https://doi.org/10.1038/s41467-020-14399-6.

[39] W. Ma, Y. Liu, S. Yan, T. Miao, S. Shi, Z. Xu, X. Zhang, C. Gao, Chemically doped macroscopic graphene fibers with significantly enhanced thermoelectric properties, Nano Res. 11 (2018) 741–750, https://doi.org/10.1007/s12274-017-1683-3.
[40] S. Foss Hansen, A. Lennquist, Carbon nanotubes added to the SIN list as a nanomaterial of Very High Concern, Nat. Nanotechnol. 15 (2020) 2–4, https://doi.org/10.1038/s41565-019-0612-x.
[41] https://sinlist.chemsec.org/.
[42] N. Pan, Unique thermal properties of clothing materials, Glob. Chall. 3 (2019) 1800082, https://doi.org/10.1002/gch2.201800082.
[43] V. Leonov, T. Torfs, P. Fiorini, C. Van Hoof, Thermoelectric converters of human warmth for self-powered wireless sensor nodes, IEEE Sensor. J. 7 (2007) 650–657, https://doi.org/10.1109/jsen.2007.894917.
[44] J.H. We, S.J. Kim, B.J. Cho, Hybrid composite of screen-printed inorganic thermoelectric film and organic conducting polymer for flexible thermoelectric power generator, Energy 73 (2014) 506–512, https://doi.org/10.1016/j.energy.2014.06.047.
[45] K. Kirihara, Q. Wei, M. Mukaida, T. Ishida, Reduction of specific contact resistance between the conducting polymer PEDOT:PSS and a metal electrode by addition of a second solvent during film formation and a post-surface treatment, Synthetic Met. 246 (2018) 289–296, https://doi.org/10.1016/j.synthmet.2018.11.005.
[46] T. Agcayazi, K. Chatterjee, A. Bozkurt, T.K. Ghosh, Flexible interconnects for electronic textiles, Adv. Mater. Technol. 3 (2018), 1700277, https://doi.org/10.1002/admt.201700277.